Analyst

PAPER

View Article Online
View Journal

Cite this: DOI: 10.1039/c3an01670f

Examining the effects of self-assembled monolayers on nanoporous gold based amperometric glucose biosensors

Xinxin Xiao,[a] Hui Li,[a] Meng'en Wang,[a] Kai Zhang*[b] and Pengchao Si*[a]

Received 4th September 2013
Accepted 26th October 2013

DOI: 10.1039/c3an01670f

www.rsc.org/analyst

Nanoporous gold (NPG) based biosensors have been constructed by covalently immobilizing glucose oxidase (GOx) onto self-assembled monolayers (SAMs). With *p*-benzoquinone (BQ) as a mediator, diffusion behavior and amperometric biosensor performance are evaluated by electrochemical characterization. The enzyme modified electrodes are demonstrated to show a thickness-sensitive behavior. Compared with planar polycrystalline gold, the unique porous structure of NPG has also been characterized *via* an electrochemical surface reconstruction process. Single-crystal gold-like electrochemical behavior on NPG and a comprehensive understanding of its impacts on sensor performance have been proposed.

1. Introduction

Vigorous efforts over the past decades have been directed towards developing rapid, sensitive, reagentless and miniaturized biosensors, especially glucose biosensors in diabetes management.[1] Coupling a biological enzyme with an electrochemical transducer is the foundation to construct bioelectronics, including biosensors[2–4] and biofuel cells.[5–8] The ideal immobilization procedure would remain biological activity of enzyme molecules, be robust enough to avoid leakage, as well as repeatable and controlled over the orientation of the enzyme.[9,10] Many appropriate methods, such as physical adsorption,[11,12] entrapment by polymers,[13,14] cross-linking with glutaraldehyde[15] and covalent binding,[16,17] have been carried out to immobilize biomolecules onto electrodes. Especially, self-assembled monolayers (SAMs) formed by alkanethiols on electrodes have been widely used as robust bridges for enzyme immobilization, with a relatively high degree control over position and loading of biomolecules.[4] Accompanied by the simplicity and adaptability of SAMs, they provide ideal platforms on the molecular level to understand the effect of different parameters on biosensors' performance and sensing mechanism.[9,16,18]

Recently, emerging of nanomaterials, including noble metal nanoparticles,[19–21] carbon nanotubes,[22] graphene[23,24] and nanoporous structure materials,[25–27] extremely enables the bio-devices to be miniaturized and enhances biosensor performance in terms of sensitivity and dynamic range due to the high specific surface area and good electrical conductivity. More recently, dealloyed nanoporous gold has been demonstrated as a promising substrate for biosensors due to its intrinsic physicochemical advantages (*e.g.* biocompatibility, support-free, tunable porosity and convenient surface functionalization *via* thiol-conjugates).[26–32] For instance, Hu *et al.* have developed a sensitive electrochemical DNA biosensor by combining NPG as a substrate with multifunctional encoded gold nanoparticles (AuNPs), which displays a limit of detection for target DNA as low as 28 aM.[33] Tan *et al.* have successfully immobilized two common proteins, bovine serum albumin (BSA) and immunoglobulin G (IgG), using *N*-hydroxysuccinimide (NHS) ester functionalized SAM on NPG in a flow-through approach.[34] Most importantly, the authors have provided important information of the distribution of immobilized protein outside and inside NPG by atomic force microscopy (AFM), which throws light on NPG based biosensors and other biological applications.[34] Chen *et al.* have recently demonstrated that glucose biosensors fabricated by covalently attaching GOx on NPG show higher sensitivity *versus* those by physical adsorption and the best performance can be acquired from NPG with 30 nm pores.[27] As increasingly NPG based biological recognition components have been developed, comprehensive characterization and understanding of the impacts of the unique porous structure on electrochemical behaviors are in demand particularly. It is notable that the effects of SAMs on NPG electrodes have not been clearly explained, which would be significant to deeply understand the electron transfer (ET) and mass transport of electroactive species in the nanochannels of NPG based biosensors.

In this paper, we fabricate glucose biosensors by wiring the GOx on the NPG surface with SAMs *via* carbodiimide chemistry. According to Marcus theory, the rate of ET is determined by parameters such as the reorganization energy and the distance

[a]*Key Laboratory for Liquid-Solid Structural Evolution and Processing of Materials, Ministry of Education, School of Materials Science and Engineering, Shandong University, Jinan 250061, People's Republic of China. E-mail: pcsi@sdu.edu.cn*
[b]*Shandong University Qilu Hospital, no. 107, Wen Hua Xi Road, Jinan, Shandong 250012, People's Republic of China. E-mail: zk0827019@sina.com*

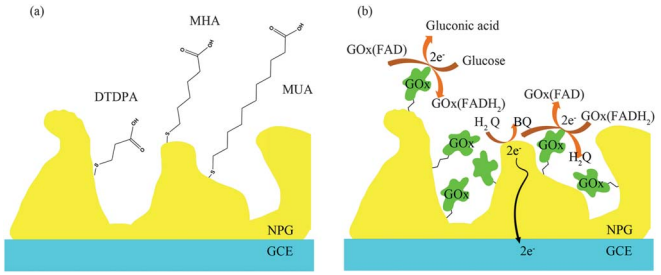

Scheme 1 Schematic illustration of DTDPA, MHA and MUA assembled on NPG (a). A possible electron transfer route on the biosensor (b).

between the donor and the acceptor.[35] This has prompted us to tune the thickness of SAMs and evaluate their impacts, adopting three types of alkanethiols with various lengths, 3,3′-dithiodipropionic acid (DTDPA), 6-mercaptohexanoic acid (MHA) and 11-mercaptoundecanoic acid (MUA) (Scheme 1a). Focused on interesting electrochemical phenomena which occur on the NPG surface due to their intrinsic structure, the electrochemical characteristics of the biosensors have been measured and compared with planar polycrystalline gold (poly-Au) based biosensors.

2. Experimental section

2.1. Chemicals

The enzyme glucose oxidase (GOx) from *Aspergillus niger* (EC 1.1.3.4, type II, ≥15 000 units per g) was purchased from Sigma-Aldrich company (Saint Louis, USA). 3,3′-Dithiodipropionic acid (DTDPA, 99%), 6-mercaptohexanoic acid (MHA, 90%) and 11-mercaptoundecanoic acid (MUA, 95%) were also purchased from Sigma-Aldrich. Sodium dihydrogen phosphate (99.99%), disodium hydrogen phosphate (99.99%), potassium perchlorate (99.99%), potassium hydroxide (KOH, 99.99%), *p*-benzoquinone (BQ, 98%), *N*-2-hydroxyethylpiperazine-*N*-2′-ethanesulfonic acid (HEPES, 99.5%), *N*-(3-dimethylaminopropyl)-*N*′-ethylcarbodiimide (EDC, 98.5%), *N*-hydroxysuccinimide (NHS, 98%) and β-D-glucose (99.5%) were supplied by Aladdin (China). Sulfuric acid (H_2SO_4, 98%) and nitric acid (HNO_3, 65%) were from Shanghai Sinopharm Chemical Co., Ltd. (Shanghai, China). Ultrapure water with a resistivity >18.25 MΩ cm^{-1} was obtained from a UPH-IV ultrapure water purifier (Chengdu Ultrapure Technology Co., Ltd, China). All chemicals were used as received without any further purification.

2.2. Fabrication of NPG electrodes

Dealloyed NPG sheets were prepared by chemically etching 100 nm-thick Au/Ag leaves (12-carat, Sepp Leaf Products, New York) in concentrated HNO_3 for 30 min at 30 °C. After carefully washing three times with ultrapure water, the free-standing NPG films were placed onto the polished glassy carbon electrodes (GCEs) with a diameter of 4 mm and stored in a desiccator to dry for at least 3 h.

2.3. Morphology characterization of NPG

The nanostructure of NPG was characterized using a Hitachi SU-70 field emission scanning electron microscope (FESEM), equipped with an energy-dispersive X-ray (EDX) analyzer for compositional analysis, and a Philips Tecnai 20U-TWIN high-resolution transmission electron microscope (HRTEM).

2.4. Fabrication of enzyme electrodes

Pretreatment of as-prepared NPG electrodes were carried out by cyclic voltammetry (CV) in 1 M H_2SO_4 to create high active surface areas. In detail, CV was applied on the electrodes between the potentials −0.2 and +1.2 V (*vs.* SCE) at a scan rate of 100 mV s^{-1} until reproducible scans were obtained (typically 20 cycles). The electrochemically activated NPG electrodes were rinsed with water before modification.

To form a particular monolayer on the NPG surface, cleaned electrodes were incubated in 10 mM DTDPA, MHA or MUA ethanolic solution for 12 h, respectively, followed by sequentially rinsing with ethanol and ultrapure water. The SAM-modified electrodes were activated by immersion in a pH 5.5 HEPES buffer solution containing 5 mM EDC and 10 mM NHS for 3 h.[36] After washing with water, the electrodes were immediately placed in an enzyme solution of 60 mg ml^{-1} GOx in phosphate buffer solution (PBS, pH 7.0) for 6 h. The resulting enzyme modified electrodes were denoted as NPG–DTDPA–GOx, NPG–MHA–GOx and NPG–MUA–GOx. For comparison, enzyme-modified poly-Au electrodes with a diameter of 3 mm were fabricated in the same way, denoted as Au–DTDPA–GOx, Au–MHA–GOx and Au–MUA–GOx, respectively. Prior to usage, the enzyme modified electrodes were soaked in 0.1 M pH 7.0 PBS.

2.5. Electrochemical measurements

A conventional three-electrode cell, which consisted of the enzyme modified NPG working electrode, a Pt wire counter electrode, and a saturated calomel reference electrode (SCE), was used for the electrochemical measurement. All potentials were reported with respect to SCE. 20 min nitrogen bubbling was used to remove oxygen from all aqueous solutions before electrochemical experiments. Cyclic voltammetry (CV) and single potential step chronoamperometry (SPSC) were performed by using a LK2005A electrochemical workstation system (Lanlike Company, Tianjin). Electrochemical reductive desorption of SAMs was performed in 0.5 M KOH solution by CV at a scan rate of 100 mV s^{-1}. Amperometric measurements of glucose were recorded under constant potentials in a 0.1 M pH 7.0 PBS containing 1 mM BQ with successive additions of 0.02 ml stock glucose solution (0.5 M).

3. Results and discussion

3.1. Morphology and electrochemical characterization of NPG

SEM and HRTEM images of NPG dealloyed by concentrated nitric acid for 30 min are illustrated in Fig. 1. NPG exhibits a bicontinuous open structure comprising ligaments and nanopores, with a pore size around 30 nm. The porous structure and biocompatibility of NPG favor enzyme loading and enhance enzyme activity and stability.[30]

CV in H_2SO_4 solution is a straightforward method to determine the active surface area of thin NPG films.[37] Total charge, calculated by integration of the cathodic peak (at ~880 mV *vs.* SCE) area, is proportional to the active area. As shown in Fig. 2A, a roughness factor (the ratio of real area to apparent area) of ~7 for the NPG is obtained, assuming that a specific charge of 390 μC cm^{-2} was required for gold oxide reduction.[37] It is notable that poly-Au only presents a single broad anodic peak from cyclic voltammograms, while well-defined anodic peaks appear in the voltammograms of NPG (Fig. 2A), which are consistent with the presence of large numbers of Au(111), Au(100) and Au(110) facets.[38] Considering this interesting phenomenon, we suggest that NPG is likely to show single-crystal gold-like electrochemical behavior, which is distinctive from poly-Au.

To verify this point by more experimental results, CV of NPG in 10 mM $KClO_4$ has been performed. As ClO_4^- shows no reaction occurring on the clean gold electrode surface during potential cycling, redox peaks obtained only belong to oxidation and reduction of gold atoms. Three evident cathodic peaks are observed in voltammograms of NPG, while only two from those of poly-Au (Fig. 2B). Three similar cathodic peaks can also be found in the voltammograms of low-index single-crystal gold faces.[39] Fingerprint featured positions and shapes of redox peaks reveal electrode surface adsorption conditions and the orientation of gold atoms on the surface.[38] These above electrochemical results show the significant distinction in the oxidation and reduction of gold itself (gold surface reconstruction), probably due to the fact that atoms on the surface of NPG are more active than those on the poly-Au surface. Atomic insights of NPG have been obtained by using a spherical-aberration-corrected TEM, through which low-index planes and monoatomic-layer islands are observed.[40]

The reductive desorption process of SAMs in alkaline solution is a suitable method to evaluate surface conditions of the metal substrate.[41] Voltammograms for reductive desorption of SAMs on poly-Au and NPG in 0.5 M KOH are shown in Fig. 3. Reduction peaks, which stem from the desorption of thiol derivatives from different surface orientations, are significantly higher and better distinguished than those of poly-Au. It has been reported that heterogeneity of binding sites, *e.g.* basal planes and stepped surfaces, determines the shape of desorption voltammetric waves.[42] The fact, combined with the above CV results, is thereby indicative of NPG possessing totally distinct surface condition compared with poly-Au. By calculation, it can be confirmed that the gold surface is not 100% occupied by thiol molecules, suggesting the existence of defects and pinholes.

3.2. Diffusion study with the freely diffusing mediator on NPG modified electrodes

Amperometric biosensors are based on generating current signals by the redox species oxidizing or reducing on the transducer surface. In the particular case of GOx, the substrate, D-β-glucose, reacts with GOx(FAD) and finally converts to gluconic acid. To recycle GOx($FADH_2$) back to GOx(FAD), redox

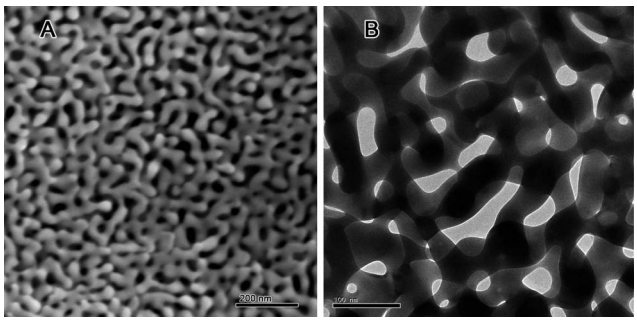

Fig. 1 SEM (A) and HRTEM (B) images of NPG.

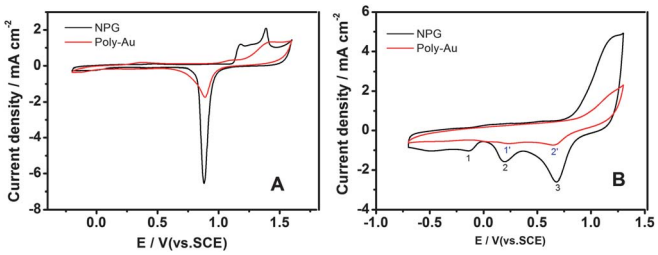

Fig. 2 Cyclic voltammograms for NPG and poly-Au in 1 M H_2SO_4 (scan rate: 100 mV s^{-1}) (A) and 10 mM $KClO_4$ (scan rate: 50 mV s^{-1}) (B).

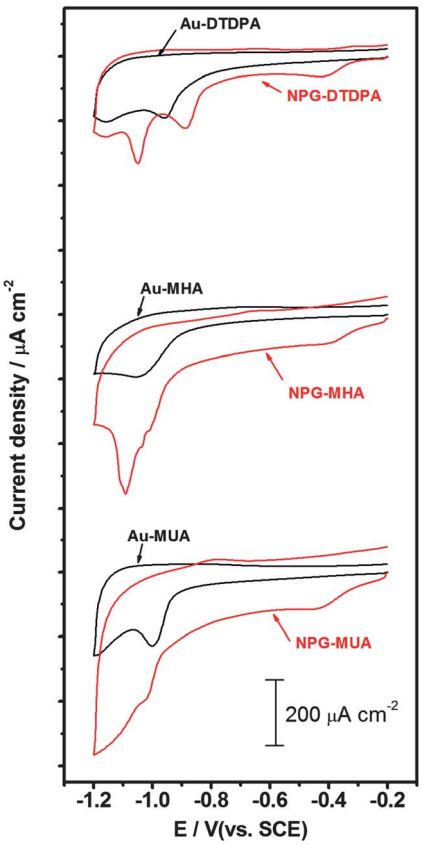

Fig. 3 Cyclic voltammograms for reductive desorption of SAMs on poly-Au and NPG in 0.5 M KOH (scan rate: 100 mV s^{-1}).

mediator (BQ) has to be reduced (1,4-hydroquinone, H_2Q); the reoxidized current of the mediator is recorded at the electrode to analyze glucose concentrations[2] (Scheme 1b). There are two routes for ET: one is mediators diffusing to the exposed electrode surface supplied by the defects and pinholes from SAMs and the other is tunneling across the molecular layer above the electrode surface.[43] The ET from the enzyme to the electrode surface, as well as mass transfer between the bulk solution and the electrode surface, is the basis of the biosensor behavior.[9]

Fig. 4 shows the cyclic voltammograms of bare planar Au, bare NPG and GOx attached electrodes in 0.1 M pH 7.0 PBS containing 1 mM BQ. A pair of oxidation and reduction peaks for BQ can be observed. Regarding both planar Au and NPG, as displayed in Table 1, peak-to-peak potential separations increase and redox peak currents decrease as the thickness of SAM increases. It can be concluded that SAM plays a role of a barrier to mass and electron transport.[44,45] Direct comparison of planar Au with NPG in the output electrochemical signal is not valid because deep inner nanopores contribute slightly to fast kinetic controlled redox reactions.[25,26] Herein it is interesting to find that curves of DTDPA and MHA assembled on planar Au are almost overlapped, while it is easy to identify them on NPG, which may be attributed to the unique active surface at NPG.

By cycling with different scan rates ranging from 50 to 1500 mV s^{-1}, anodic and cathodic peak currents are linearly proportional to the square root of scan rates, as plotted in Fig. 5, revealing a diffusion-controlled ET process according to Randles–Sevcik equation:[46]

$$I_p = 2.69 \times 10^5 n^{3/2} A D^{1/2} C \nu^{1/2} \quad (1)$$

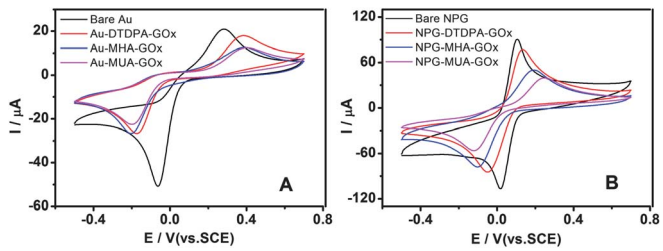

Fig. 4 Cyclic voltammograms of bare Au, Au–DTDPA–GOx, Au–MUA–GOx, bare NPG, NPG–DTDPA–GOx and NPG–MUA–GOx in 0.1 M pH 7.0 PBS containing 1 mM BQ. Scan rate: 50 mV s^{-1}.

Table 1 Electrochemical behavior comparison of different electrodes

Electrode	E_{pa} (mV)	E_{pc} (mV)	ΔE_p (mV)
Bare Au	284.0	−64.0	348.0
Au–DTDPA–GOx	383.3	−173.3	556.6
Au–MHA–GOx	390.0	−191.0	581.0
Au–MUA–GOx	401.2	−199.3	600.5
Bare NPG	104.0	18.0	86.0
NPG–DTDPA–GOx	133.6	−50.2	183.8
NPG–MHA–GOx	192.0	−102.0	294.0
NPG–MUA–GOx	248.6	−118.6	367.2

where I_p is the peak current, n is the number of electrons transferred, A is the electrode area, C is the concentration of BQ and ν is the scan rate, considering a temperature of 298 K. As shown in Table 2, slopes of I_p *vs.* $\nu^{1/2}$ decrease gradually since SAM gets thicker, indicating worse diffusion of BQ. It can be explained that as the alkyl chain length increases, along with the increase of van der Waals interactions between chains, the SAM prefers to adopt a more compact conformation[47] and reduces diffusion coefficient consequently.

Unlike the planar electrode, the nanoporous electrode shows unique features, including an electrical double layer (EDL) profile, electric field within the pores, and Knudsen diffusion.[48] In this case, EDL has no effect on mass transport, as BQ is electrically neutral. Knudsen diffusion is helpful to understand why the electrode surface is more accessible for molecules within nano-confined space. Our results are consistent with the model. When SAMs are the same, NPG based electrodes demonstrated better diffusion conditions than those of poly-Au.

Another aspect taken into consideration is the ET from the enzyme to the electrode surface. A model of distance dependent electron tunneling through SAMs has been proposed by D. J. Wold *et al.*,[49] providing a quantitative perspective to evaluate the ET process. Resistance, R, is expressed as:

$$R = R_0 \exp(Bs) \quad (2)$$

where R_0, B, and s represent the effective contact resistance, the structure-dependent factor which relates to bonding and functional group patterns in the molecules, and the molecular length. R increases exponentially to s, suggesting that the slightly increase of SAM thickness would greatly resist electron tunneling. As for planar gold, B can be simplified to be 1.16 per methylene unit,[50] and the s values of DTDPA, MHA and MUA, indicated in terms of the number of methylene groups, correspond to 2, 5 and 10, respectively. From these parameters, the relative conductivity can be calculated as DTDPA : MHA : MUA = 1 : 32 : 3361. Although the coherent electron tunneling mechanism does not dominate the diffusion-controlled process here, it is helpful for us to understand this thickness-sensitive behavior. The conductivity of alkanethiolate-passivated gold nanoparticles has been estimated to be a few orders of magnitude smaller than that of bulk gold.[51] Due to its active surface, NPG is supposed to accelerate electron tunneling through SAMs, but the values of B, suggested to be smaller than those on planar gold, for alkanethiols on NPG surfaces, remain to be researched by scanning probe microscopy.

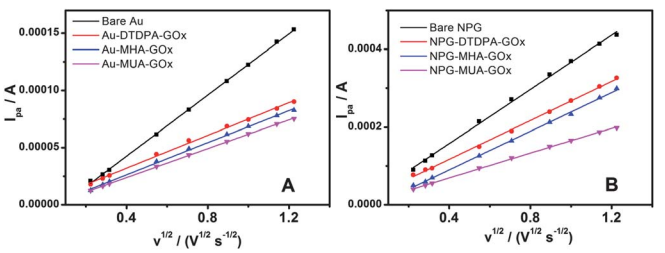

Fig. 5 Plot of the anodic peak current *versus* the square root of scan rate.

Table 2 The slope of I_p *vs.* $\nu^{1/2}$ plot of different electrodes (calculation to anodic currents by Randles–Sevcik equation)

Electrode	Slope (A $s^{1/2}$ $V^{-1/2}$)	Electrode	Slope (A $s^{1/2}$ $V^{-1/2}$)
Bare Au	1.34×10^{-4}	Bare NPG	3.49×10^{-4}
Au–DTDPA–GOx	7.17×10^{-5}	NPG–DTDPA–GOx	2.51×10^{-4}
Au–MHA–GOx	7.02×10^{-5}	NPG–MHA–GOx	2.49×10^{-4}
Au–MUA–GOx	6.32×10^{-5}	NPG–MUA–GOx	1.59×10^{-4}

3.3. Comparative amperometric response of the biosensors

Typical amperometric responses of as-fabricated glucose biosensors on successive step changes of glucose concentrations are performed. Inspired from CV results in Fig. 4, the detection potential is +0.4 V for planar Au based electrodes and +0.2 V for NPG. In contrast to poly-Au based electrodes, NPG based electrodes show faster response time to reach 90% of the steady state,[52] indicating excellent electrocatalytic and diffusive behavior.

Fig. 6 shows calibrations of the biosensors by plotting steady-state currents *vs.* glucose concentrations, demonstrating linear relationships in the range between 1 mM and 10 mM. A sensitivity of 0.672 μA mM^{-1} cm^{-2} for Au–DTDPA–GOx is at comparable scales to a similar constructed biosensor with a sensitivity of 0.41 μA mM^{-1} cm^{-2}, reported by J. J. Gooding *et al.*[10] Besides the lower detection potential, sensitivities of NPG based biosensors are several times better than those of planar Au, indicating NPG as an ideal candidate for biosensing applications.[27]

As shown in Table 3, the sensitivity decreases as the chain length increases. In other words, the performance of the SAM bridged biosensors is sensitive to the thin film thickness in the situation of the diffusion-controlled ET procedure, which coincided well with the CV results. Similar points are also concluded by investigating glucose biosensors based on SAM and Prussian blue hybrid system.[53] SAMs with longer carbon chains seem to be denser, resulting in more enzymes immobilized, whereas ET becomes more difficult at the same time due to the passivated transduction interface, resulting in lower sensor sensitivity.[54]

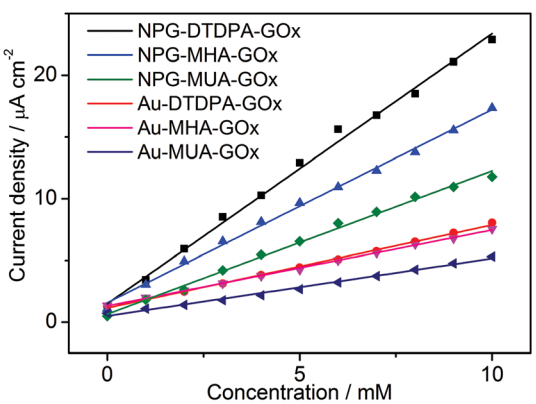

Fig. 6 Calibration plots for Au–DTDPA–GOx, Au–MHA–GOx, Au–MUA–GOx, NPG–DTDPA–GOx, NPG–MHA–GOx and NPG–MUA–GOx sensors.

Table 3 Performance comparison of different enzyme modified electrodes

Electrode	Sensitivity (μA mM^{-1} cm^{-2})	RSD[a] (%)
Au–DTDPA–GOx	0.672	2.06
Au–MHA–GOx	0.615	1.57
Au–MUA–GOx	0.465	2.52
NPG–DTDPA–GOx	2.187	2.11
NPG–MHA–GOx	1.564	4.45
NPG–MUA–GOx	1.160	0.09

[a] Obtained by three repeated determinations.

Table 4 Glucose detection in human serum samples

Sample	Biochemical analyzer (mM)	NPG–DTDPA–GOx[a] (mM)	RSD (%)
1	4.40	4.62	1.50
2	4.36	4.31	2.01
3	4.89	4.80	0.16

[a] Each sample has been measured in triplicate.

3.4. Determination of glucose in human serum samples

In order to verify the practical application of the biosensor in clinical analysis, the NPG–DTDPA–GOx electrode has been selected to measure glucose in human serum samples with a 50-fold dilution in the presence of 1 mM BQ at +0.2 V. The calculated results are compared with those measured using a biochemical analyzer (Cobas 8000 analyzer, Roche Diagnostics, Germany) in Table 4. The results are in an acceptable agreement with the data from the commercial analyzer, indicating that the proposed biosensor is applicable in real human sample analysis.

4. Conclusions

In the present work, a SAM bridge strategy has been used to fabricate NPG based thin film amperometric glucose biosensors. Comparatively examining the effects of SAM film thickness on mass transfer and sensor performance has been carried on. The performance is supposed to be sensitive to the SAM thickness. Electrochemical evidence presented here is in support of the existence of unique high active surface planes on NPG electrodes, which also affect sensor behaviors. Compared with planar polycrystalline gold, NPG exhibits unique electrochemical characteristics such as possessing inner electroactive

crystal planes and enhanced electron and mass transfer, resulting in lower detection potential, decreased response time and higher sensitivity, indicating an ideal platform for enzyme immobilization.

Acknowledgements

This work is sponsored by the National 973 (2012CB932800) Program Project of China, Shandong Provincial Natural Science Foundation (Q2008C08), Independent Innovation Foundation of Shandong University (IIFSDU-2012TS159), no. 31370056431211 and no. 31370070614018(2010TB018) project from Shandong University. We also appreciate Prof. Yi Ding for his kind support.

References

1 A. Heller and B. Feldman, *Chem. Rev.*, 2008, **108**, 2482–2505.
2 J. Wang, *Chem. Rev.*, 2008, **108**, 814–825.
3 G. S. Wilson and Y. Hu, *Chem. Rev.*, 2000, **100**, 2693–2704.
4 J. J. Gooding and N. Darwish, *Chem. Rec.*, 2012, **12**, 92–105.
5 S. C. Barton, J. Gallaway and P. Atanassov, *Chem. Rev.*, 2004, **104**, 4867–4886.
6 L. Halamkova, J. Halamek, V. Bocharova, A. Szczupak, L. Alfonta and E. Katz, *J. Am. Chem. Soc.*, 2012, **134**, 5040–5043.
7 A. Zebda, C. Gondran, A. Le Goff, M. Holzinger, P. Cinquin and S. Cosnier, *Nat. Commun.*, 2011, **2**, 370.
8 I. Willner, Y. M. Yan, B. Willner and R. Tel-Vered, *Fuel Cells*, 2009, **9**, 7–24.
9 J. J. Gooding and D. B. Hibbert, *Trends Anal. Chem.*, 1999, **18**, 525–533.
10 J. J. Gooding, L. Pugliano, D. B. Hibbert and P. Erokhin, *Electrochem. Commun.*, 2000, **2**, 217–221.
11 Y. Y. Sun, Y. Bai, W. W. Yang and C. Q. Sun, *Electrochim. Acta*, 2007, **52**, 7352–7361.
12 X. H. Pham, M. P. Bui, C. A. Li, K. N. Han, J. H. Kim, H. Won and G. H. Seong, *Anal. Chim. Acta*, 2010, **671**, 36–40.
13 M. Gerarda, A. Chaubeyb and B. D. Malhotrab, *Biosens. Bioelectron.*, 2002, **17**, 345–359.
14 M. Moyo, J. O. Okonkwo and N. M. Agyei, *Sensors*, 2012, **12**, 923–953.
15 I. Willner, M. Lion-Dagan, S. Marx-Tibbon and E. Katz, *J. Am. Chem. Soc.*, 1995, **117**, 6581–6592.
16 I. Willner, A. Riklin, B. Shoham, D. Rivenzon and E. Katz, *Adv. Mater.*, 1993, **5**, 912–915.
17 Y. Xiao, F. Patolsky, E. Katz, J. F. Hainfeld and I. Willner, *Science*, 2003, **299**, 1877–1881.
18 I. Willner, E. Katz, A. Riklin and R. Kasher, *J. Am. Chem. Soc.*, 1992, **114**, 10965–10966.
19 L. Deng, Y. Wang, L. Shang, D. Wen, F. Wang and S. Dong, *Biosens. Bioelectron.*, 2008, **24**, 957–963.
20 R. S. Dey and C. R. Raj, *J. Phys. Chem. C*, 2010, **114**, 21427–21433.
21 Y. M. Yan, R. Tel-Vered, O. Yehezkeli, Z. Cheglakov and I. Willner, *Adv. Mater.*, 2008, **20**, 2365–2370.
22 A. K. Sarma, P. Vatsyayan, P. Goswami and S. D. Minteer, *Biosens. Bioelectron.*, 2009, **24**, 2313–2322.
23 K. F. Zhou, Y. H. Zhu, X. L. Yang and C. Z. Li, *Electroanalysis*, 2010, **22**, 259–264.
24 C. S. Shan, H. F. Yang, J. F. Song, D. X. Han, A. Ivaska and L. Niu, *Anal. Chem.*, 2008, **81**, 2378–2382.
25 R. Szamocki, S. Reculusa, S. Ravaine, P. N. Bartlett, A. Kuhn and R. Hempelmann, *Angew. Chem., Int. Ed.*, 2006, **45**, 1317–1321.
26 M. D. Scanlon, U. Salaj-Kosla, S. Belochapkine, D. MacAodha, D. Leech, Y. Ding and E. Magner, *Langmuir*, 2012, **28**, 2251–2261.
27 L. Y. Chen, T. Fujita and M. W. Chen, *Electrochim. Acta*, 2012, **67**, 1–5.
28 M. Hakamada, M. Takahashi and M. Mabuchi, *Gold Bull.*, 2011, **45**, 9–15.
29 O. V. Shulga, K. Jefferson, A. R. Khan, V. T. D'Souza, J. Y. Liu, A. V. Demchenko and K. J. Stine, *Chem. Mater.*, 2007, **19**, 3902–3911.
30 X. Wang, X. Y. Liu, X. L. Yan, P. Zhao, Y. Ding and P. Xu, *PLoS One*, 2011, **6**, e24207.
31 Y. Ding and M. W. Chen, *MRS Bull.*, 2009, **34**, 569–576.
32 X. Xiao, M. e. Wang, H. Li and P. Si, *Talanta*, 2013, **115**, 1054.
33 K. Hu, D. Lan, X. Li and S. Zhang, *Anal. Chem.*, 2008, **80**, 9124–9130.
34 Y. H. Tan, J. R. Schallom, N. V. Ganesh, K. Fujikawa, A. V. Demchenko and K. J. Stine, *Nanoscale*, 2011, **3**, 3395–3407.
35 R. A. Marcus, *Angew. Chem., Int. Ed.*, 1993, **32**, 1111–1121.
36 J. J. Gooding, E. A. H. Hall and D. B. Hibbert, *J. Electroanal. Chem.*, 1998, **10**, 1130–1136.
37 S. Trasatti and O. A. Petrii, *Pure Appl. Chem.*, 1991, **63**, 711–734.
38 A. Hamelin, *J. Electroanal. Chem.*, 1996, **407**, 1–11.
39 C. Engelbrekt, K. H. Sørensen, J. Zhang, A. C. Welinder, P. S. Jensen and J. Ulstrup, *J. Mater. Chem.*, 2009, **19**, 7839–7847.
40 T. Fujita, P. F. Guan, K. McKenna, X. Y. Lang, A. Hirata, L. Zhang, T. Tokunaga, S. Arai, Y. Yamamoto, N. Tanaka, Y. Ishikawa, N. Asao, Y. Yamamoto, J. Erlebacher and M. W. Chen, *Nat. Mater.*, 2012, **11**, 775–780.
41 M. M. Walczak, D. D. Popenoe, R. S. Deinhammer, B. D. Lamp, C. Chung and M. D. Porter, *Langmuir*, 1991, **7**, 2687–2693.
42 M. M. Walczak, C. A. Alves, B. D. Lamp and M. D. Porter, *J. Electroanal. Chem.*, 1995, **396**, 103–114.
43 N. K. Chaki and K. Vijayamohanan, *Biosens. Bioelectron.*, 2002, **17**, 1–12.
44 X. D. Dong, J. T. Lu and C. S. Cha, *Bioelectrochem. Bioenerg.*, 1995, **36**, 73–76.
45 J. J. Gooding, V. G. Praig and E. A. H. Hall, *Anal. Chem.*, 1998, **70**, 2396–2402.
46 A. J. Bard and L. R. Faulkner, *Electrochemical Methods: Fundamental and Applications*, John Wiley & Sons Inc., New York, 2001.

47 F. P. Cometto, C. A. Calderón, E. M. Euti, D. K. Jacquelín, M. A. Pérez, E. M. Patrito and V. A. Macagno, *J. Electroanal. Chem.*, 2011, **661**, 90–99.
48 J. H. Bae, J. H. Han and T. D. Chung, *Phys. Chem. Chem. Phys.*, 2012, **14**, 448–463.
49 D. J. Wold, R. Haag, M. A. Rampi and C. D. Frisbie, *J. Phys. Chem. B*, 2002, **106**, 2813–2816.
50 C. R. Bradbury, J. Zhao and D. J. Fermín, *J. Phys. Chem. C*, 2008, **112**, 10153–10160.
51 S. Chen, *Anal. Chim. Acta*, 2003, **496**, 29–37.
52 D. R. Thévenota, K. Tothb, R. A. Durstc and G. S. Wilsond, *Biosens. Bioelectron.*, 2001, **16**, 121–131.
53 H. H. Wang, H. Ohnuki, H. Endo and M. Izumi, *Sens. Actuators, B*, 2012, **168**, 249–255.
54 R. K. Mendes, R. F. Carvalhal and L. T. Kubota, *J. Electroanal. Chem.*, 2008, **612**, 164–172.